Li, Z; Chang, Y; Rong, J; Min, J; Lian, J

# Edge fracture of the first and third-generation high-strength steels : DP1000 and QP1000

*Published in:*
IOP Conference Series: Materials Science and Engineering

*DOI:*
10.1088/1757-899X/1284/1/012021

Published: 01/01/2023

*Document Version*
Publisher's PDF, also known as Version of record

**PAPER** • **OPEN ACCESS**

# Edge fracture of the first and third-generation high-strength steels: DP1000 and QP1000

To cite this article: Z Li *et al* 2023 *IOP Conf. Ser.: Mater. Sci. Eng.* **1284** 012021



# Edge fracture of the first and third-generation high-strength steels: DP1000 and QP1000

**Z Li[1], Y Chang[2], J Rong[1], J Min[3] and J Lian[1]***

[1] Department of Mechanical Engineering, Aalto University, 02150 Espoo, Finland
[2] Steel Institute, RWTH Aachen University, Intzestraße 1, 52072 Aachen, Germany
[3] School of Mechanical Engineering, Tongji University, Shanghai 201804, China

E-mail: junhe.lian@aalto.fi

**Abstract**. Advanced high-strength steels (AHSS) have shown profound progress in improving tensile ductility or global formality in the last decades over three generations. For a complete assessment of both the global and local formability, this study aims to characterize and compare the tensile and edge fracture behavior of the first and third-generation AHSS (dual-phase steel and quenching & partitioning steel) with the same nominal strength level of 980 MPa. Uniaxial tensile tests are performed to characterize the tensile properties. Hole expansion tests are conducted with two edge conditions based on separated preparation techniques (waterjet with polishing and punching) to investigate the edge fracture for both materials. The hole expansion ratios and edge fractures are compared between two materials and two edge conditions. It is concluded that the investigated QP1000 has promoted global formability while the DP1000 shows better local formability due to its damage-tolerant and crack-resistant responses.

## 1. Introduction

Advanced high-strength steels (AHSS) were developed in the automotive industries to improve crashworthiness and lightweight structure [1]. The first-generation (1$^{st}$ G) AHSS elevates the strength level beyond 800 MPa from traditional high-strength steels, whereas the superior strength comes with the sacrifice of ductility. Among the widely adopted grades, dual-phase (DP) steels are the most popular and developed ones, due to their balanced properties of high strength, good strain hardening, and low production cost [2]. Those steels are commonly used to produce complex parts from numerous manufacturing processes, in which the formability of the material becomes vital to be evaluated. Formability is assessed from two aspects, global and local. Global formability is sufficient to describe the necking limit of the sheet material in the global forming modes, such as stretching, drawing, and plane-strain tension, where the deformation of the material is distributed evenly over a relatively large region. Whereas the local formability is determined by the fracture limit when concentrated deformation occurs locally in the local forming modes including bending, collar forming, and hole expansion. Among all global and local failures, edge fracture tends to be extremely critical since the edge formability is depending on both material properties and the edge quality.

Numerous studies have been conducted to characterize both the local and global formability [3-8] of DP steels. In the meanwhile, the third-generation (3$^{rd}$ G) steels were proposed [9] with specific processes. One typical example is the Quenching and Partitioning (QP) steels, offering a superior combination of strength and ductility, which is significantly promoted from the 1$^{st}$ G. QP 1000 grades and relatively novel with improved global formability [10]. It is still under evaluation for many applications, e.g., in manufacturing structural parts such as bumpers and B-pillars, where the edge area undergoes large deformation, usually at uniaxial tension, plane-strain tension, or rather complex stress states. However, when it comes to the local formability, especially the stretch-flange-ability of the edge, the investigation is quite limited.

To accurately characterize the stretch-flange-ability of the edge, a variety of experimental methods have been reported [11]. Among them, the hole expansion test (HET) is a commonly used method to effectively evaluate the stretchability of sheet metal and its edge fracture [12-14]. It is verified that HET gives good results in characterizing the edge crack sensitivity of AHSS steels [15]. Different influencing factors have been studied for DP and complex-phase (CP) steels to find out the most critical ones [16]. As reported in a large number of studies, the severe pre-damage introduced to the hole edge by the blanking process in the shear-affected zone (SAZ), places a dominating role in the edge stretch-flange-ability. It is verified that HET gives good results in characterizing the edge crack sensitivity of AHSS steels [15]. Different influencing factors have been studied for DP and complex-phase (CP) steels to find out the most critical ones [16]. As reported in a large number of studies, the severe pre-damage introduced to the hole edge by the blanking process in the shear-affected zone (SAZ), places a dominating role in the edge stretch-flange-ability [17-19]. The edge effect therefore must be taken into consideration for edge formability. Madrid et al. [20] reported QP1000 is not sensitive to the punch geometry. Goshert et al. [21] studied four edge conditions with angular stretch bend tests for QP980 and DP600, which emphasized the influence of edge effects. Nevertheless, there are few comparative studies regarding the local formability between the 1st and 3rd Gen. steels [22], and particularly no data is available for QP1000 and DP1000 in the current literature.

Therefore, in the current study, uniaxial tensile and hole expansion tests are conducted to investigate the tensile and edge fracture behavior of QP1000 and DP1000. Two conditions for smooth and blanked edges based on different forming methods including waterjet cutting with polishing and punching, are prepared. After hole expansion tests, the edge fracture patterns are then characterized, followed by a damage mechanism analysis for both materials.

## 2. Materials and experiments

The sheet metals chosen for this study are as-received high-strength DP steel (DP1000) with a measured thickness of 1.46 mm and quenching & partitioning steel (QP1000) with a thickness of 1.36 mm. The chemical composition of the DP1000 and QP1000 material is performed via a BELEC LAB 3000s optical emission spectrometer. The analysis results are summarized in Table 1. The microstructure was obtained from scanning electron microscopy (SEM). The micrographs of both materials are shown in Figure 1. DP1000 is composed of ferrite and martensite phases, with an approximate martensite phase fraction of 45% [23]. QP1000 contains metastable retained austenite (RA), tempered martensite, secondary martensite, as well as non-martensitic constituents (NMC) such as bainitic ferrite apart from ferrite.

**Table 1.** Chemical composition of DP1000 and QP1000 (mass content in %).

| Material | C | Si | Mn | Al | P | S | Ti + Nb | Cr + Mo |
|---|---|---|---|---|---|---|---|---|
| DP1000 | 0.07 | 0.30 | 2.55 | 0.05 | <0.040 | <0.010 | <0.15 | <1.0 |
| QP1000 | 0.15 | 1.67 | 2.42 | 0.074 | <0.002 | <0.002 | 0.011 | <0.03 |

The tensile properties were tested using a Zwick/Roell Z020 screw-driven tensile machine. Uniaxial tensile tests of the smooth dog-bone (SDB) specimens were performed at room temperature (RT, 25°C) under quasi-static (QS, $10^{-4}$ $s^{-1}$) loading along rolling direction (RD). The testing setup is shown in Figure 2. A stereo digital image correlation (DIC) system was used to measure the displacement during the deformation, with the detecting camera resolution of 50 pixels/mm. To ensure the image quality, the surface of the specimen was lacquered with an even layer of white paint and then sprayed to form speckle patterns with a speckle diameter of 5-10 pixels. A parallel filter was placed before the spotlight, which can minimize the reflections from the material surface and therefore, improve the lighting condition.

Observations were recorded from Hikvision cameras with two separate signals (Left-0, Right-1) from both sides.

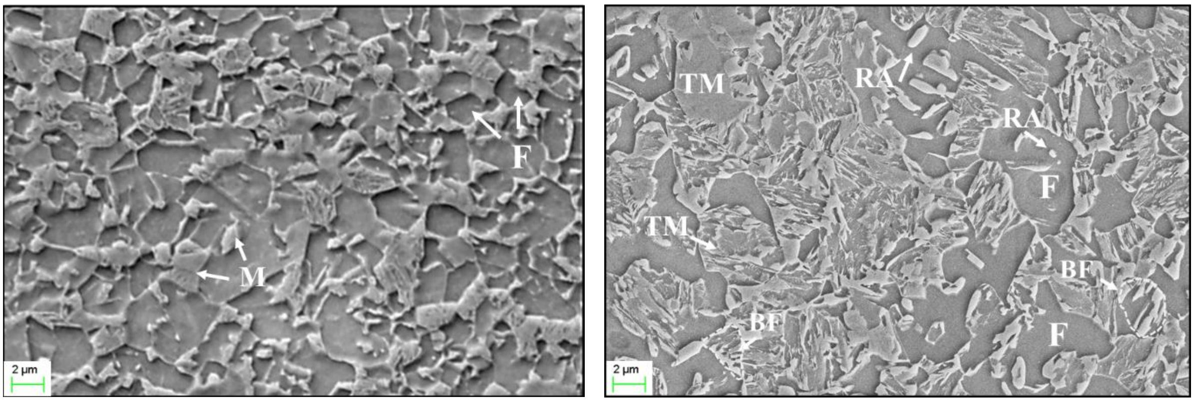


(a) (b)

**Figure 1.** Microstructure of (a) DP1000 [24] with martensite (M) and ferrite (F) phases indicated, and (b) QP1000 with retained austenite (RA), tempered martensite (TM), bainitic ferrite (BF) phases indicated.

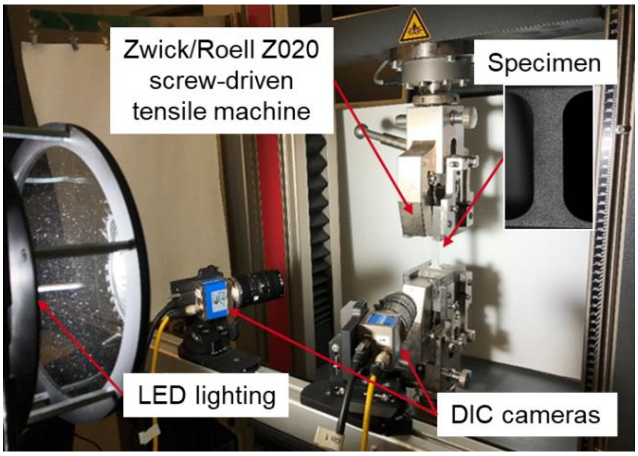


**Figure 2.** Uniaxial tensile testing set-up with stereo-DIC system and lighting.

To characterize the edge fracture, circular specimens with a diameter of 90 mm were cut as shown in Figure 3 (a). Central holes with separated edge conditions were prepared based on different manufacturing techniques. The smooth edge condition was introduced by waterjet cutting and then ground to 10 mm with a smooth finish. The blanked hole is punched from the hole blanking process as schematically illustrated in Figure 3 (b). Then these two materials under both edge conditions were conducted in the HET following the ISO/16630:2017-09 standard. The set-up of the HET is depicted in Figure 3 (c). The specimen was clamped in between the die and blank holder under a holding force of 235 kN. Then the specimen was expanded by a conical punch at a 5 mm/min expansion speed until the first through-thickness crack ($1^{st}$ TTC) was detected on the edge of the hole. The tracking of the first through-thickness crack easily got overshot with bare eyes. Therefore, a camera was introduced to record the images and observe the deformation at each frame. The hole expansion ratio (HER), as a criterion to characterize the resistance to edge fracture, was then calculated as defined in Eq. (1), where $d_h$ is the inner hole diameter after expansion and $d_0$ is the original hole diameter before the test. Both were measured by digital caliper and averaged across three repeats. The results after expansion were further verified with the measured values from the images captured by the camera, to make sure the diameters were taken at the exact time when the first through-thickness crack occurred.

$$HER = \frac{d_h - d_0}{d_0} \times 100\% \quad (1)$$

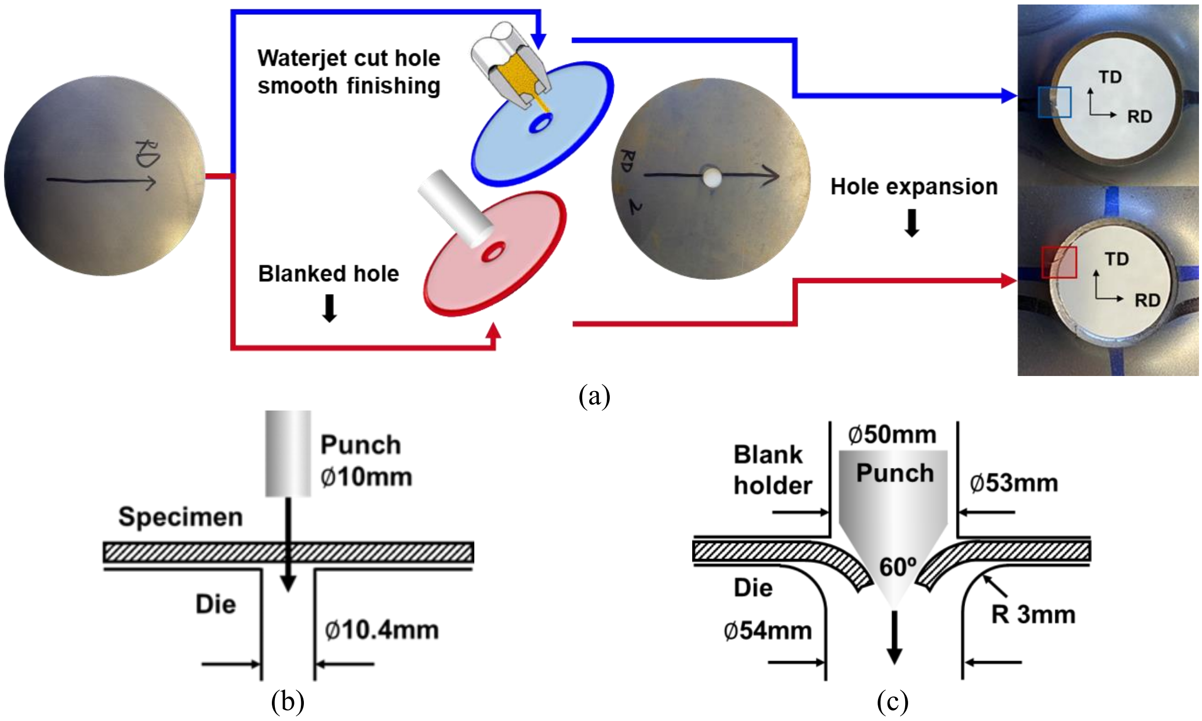


**Figure 3.** Schematic diagram of (a) the edge fracture characterization approach, (b) cross-section view of the hole blanking, and (c) cross-section view of the hole expansion process.

## 3. Results and discussion

### *3.1. Tensile properties*

The engineering stress-strain, true stress-strain, r-value, and forming limit curves from the uniaxial tensile tests along RD for both materials are shown in Figure 4. The mechanical properties of the DP and QP steels such as yield strength (YS), ultimate tensile strength (UTS), percentage uniform elongation (% UE), percentage total elongation (% TE), and Lankford coefficients (r-value) at UE are listed in Table 2. DP1000 shows a slightly higher YS value, while QP1000 surpasses UTS. From the results, QP1000 reaches yield strength sooner before DP1000, while it takes much longer elongation to reach UTS and then to fracture. The UTS is improved by 10% from DP1000 to QP1000. What is significantly enhanced is the ductility, the UE of QP1000 is more than three times higher than the one in DP1000, and the fracture elongation is also increased by more than 100%. There is no significant difference between the two materials in terms of the r-value and their evolution pattern. Further investigation can be made by taking into account the loading effect for the anisotropic properties, Further investigation can be made by taking into account the loading effect for the anisotropic properties, which can be found in detail in a follow-up study [25].

**Table 2.** Tensile properties of DP1000 and QP1000.

| Material | YS, MPa | UTS, MPa | UE, % | TE, % | R-value at UE, - |
|---|---|---|---|---|---|
| DP1000 | 770.00 | 983.38 | 5.22 | 10.97 | 0.73 |
| QP1000 | 752.20 | 1090.20 | 18.09 | 23.57 | 0.75 |

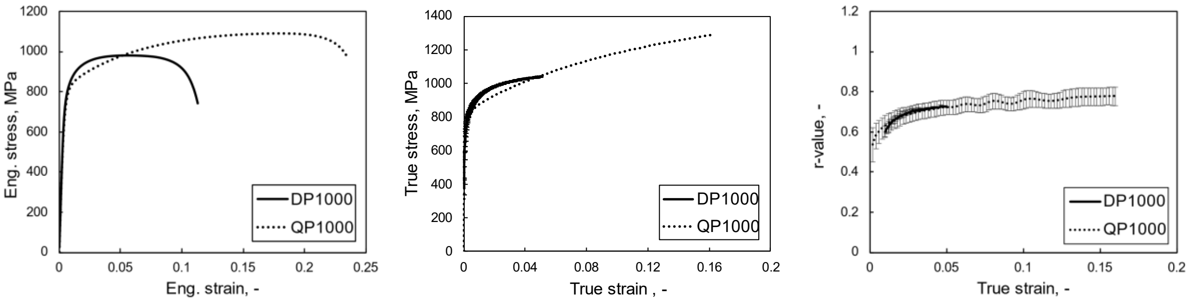


(a) (b) (c)

**Figure 4.** The tensile properties from uniaxial tensile tests, (a) engineering stress-strain curves, (b) true stress-strain curves, and (c) r-value curves of QP1000 in comparison with DP1000.

### *3.2. Edge fracture behavior*

*3.2.1. HER.* The HER values for the blanked and machined holes of DP1000 and QP1000 are compared in Figure 5 (a). Sensitivity to the edge condition for both materials was characterized by comparing the HER on each condition. Both steels demonstrate strong sensitivity to the edge condition. The HER value for DP1000 is higher than QP1000 for both conditions, i.e., DP1000 shows higher edge fracture resistance than QP1000. For the DP1000 machined hole, the HER is 92%, which is almost one and a half times the value measured for the machined hole of QP1000, 62%. A similar trend exists for the blanked hole of DP1000, which has an HER of 29%, while the HER for the blanked hole of QP1000 is 21%, giving a slightly reduced difference in between. The confidence interval has a rather small value for the blanked holes, suggesting there is no significant variation for the pre-damage introduced to the blanked edges. Whereas the error for machined holes is comparatively high, which indicates the ideal smooth condition can be easily breached, adding up the fact that it is often difficult to accurately track down the moment when the first through-thickness crack is forming. The measured HER includes error from overshoot of the punch head. As shown in Figure 5 (b) with the blue and red bars, both materials can be clearly differentiated between the edge conditions with formability reductions of 66-68%. The variations for machined holes in DP1000 are larger than in QP1000 due to the fact that the specimen preparation process is slightly different, with QP1000 cut directly from electrical discharge machining (EDM) with higher surface quality. The formability reduction for DP1000 is slightly higher than in QP1000 can be explained by the study [26] that for blanked edges, a higher density of voids can be found at ferrite-martensite interfaces. The excellent damage tolerance and crack resistance of DP1000 got depressed, making it more vulnerable to fracture. The formability distinguishes between QP1000 and DP1000 are around 27% for smooth edges as shown in a green bar, and 33% for blanked edges plotted in an orange bar.

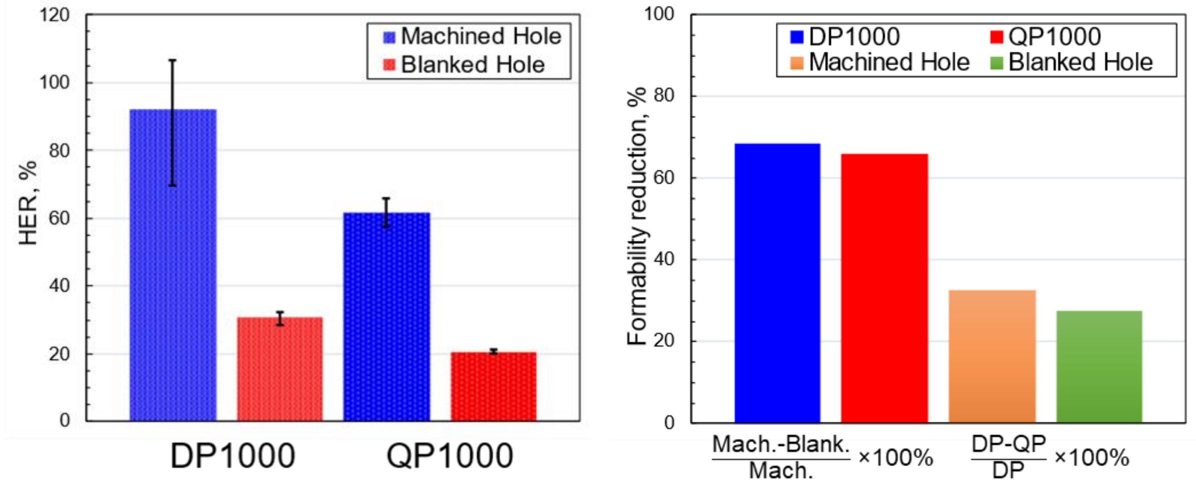


(a) (b)

**Figure 5.** HER values analysis (a) of the punched and machined holes for DP1000 and QP1000, (b) the formability reduction from smooth edge to punched edge for each material, and from DP1000 to QP1000 for each edge condition.

*3.2.2. Edge fracture on smooth holes.* The edge crack distribution and pattern for DP1000 and QP1000 on smooth holes are shown in Figure 6 and Figure 7, respectively. The localized necking is clearly observed at the hole edge close to RD in DP1000 as marked in Figure 6 (a), whereas no obvious thickness reduction can be found on the hole circumference for QP1000. As shown in Figure 6 (b), the first through-thickness crack locates near RD, with fractures prone to a slant angle of conical punch during deformation, then rapidly propagating through the thickness to form the first major crack. If the test is not halted immediately, the crack would expand further in the radial direction following a serrated path as sketched in Figure 6 (c). For QP1000, after the first major crack, a limited number of minor cracks can be observed initiating from the bottom layer, as blue triangles annotated in Figure 7. One out of all the minor cracks can also develop further to form another through-thickness crack, whereas the same behavior is not observed on DP1000. Fracture is prone to develop into one or at most two major cracks in the smooth edge region for both materials.

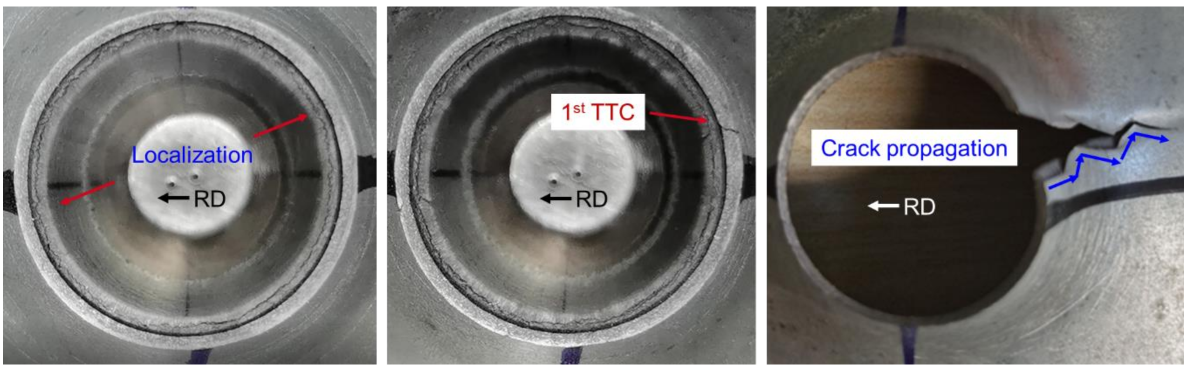


(a) (b) (c)

**Figure 6.** Edge fracture pattern and locations on smooth edges for DP1000 (a) after strong localization, (b) the moment when the first through-thickness crack occurs, and (c) crack propagation with blue marks.

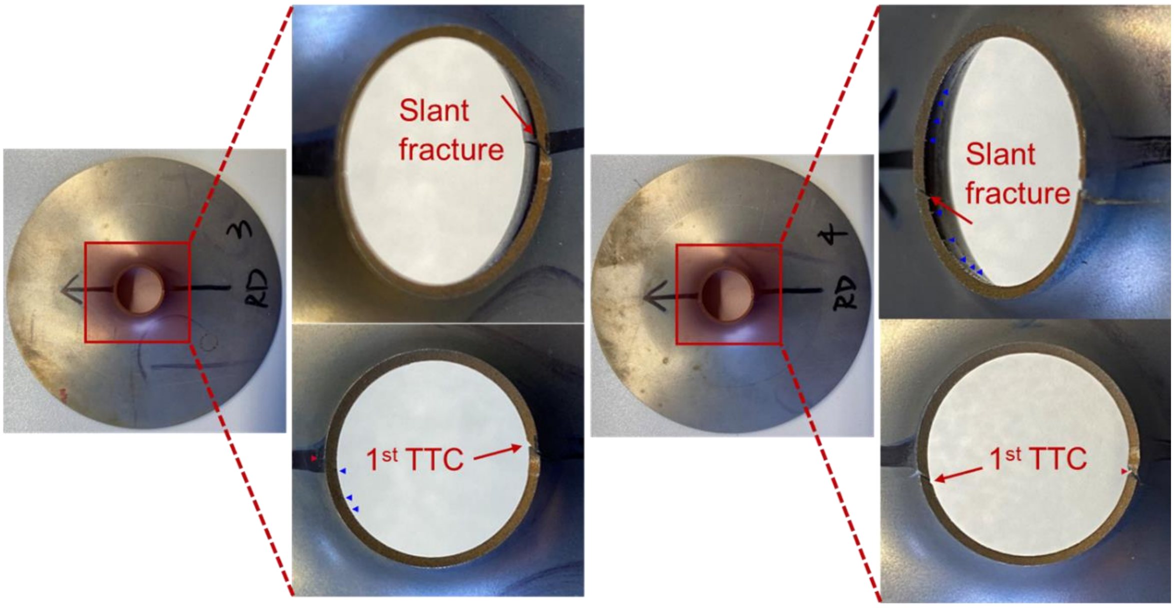


**Figure 7.** Edge fracture pattern and locations on smooth edges for QP1000 after first through-thickness crack, and blue marks for minor cracks.

*3.2.3. Edge fracture on punched holes.* The edge crack distribution and pattern for DP1000 and QP1000 on punched holes are shown in Figure 8 (a) and (b), respectively. No noticeable localization can be witnessed for either material. The first through-thickness crack has the same location close to RD as in smooth edges, while the fractures were prone to a slant angle of 45º. Different from the pattern on the smooth edge, the crack initiates not only from the bottom layer but also from the top surface of the punched hole. The number of minor cracks on punched edges is distinctively larger than in the smooth condition for both materials, while DP1000 collects more minor cracks than QP1000. When the force is applied continuously after the first major crack appears, the hole gets expanded further. For DP1000, the number of major cracks grows to four. The location of these four major cracks at the open-up circumference is along RD and transverse direction (TD), as marked with red circles in Figure 8 (c). For QP1000, the number of major cracks ended into six as shown in Figure 8 (d). The locations are not only at RD, and TD but also along the diagonal direction (DD).

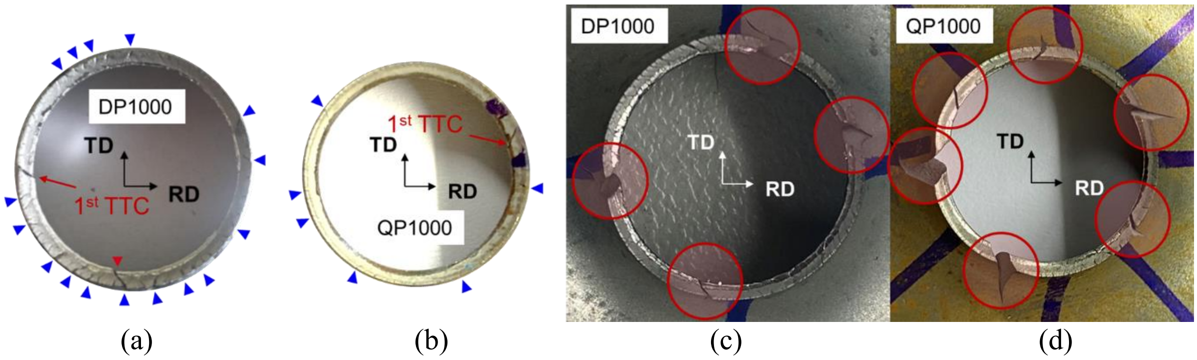


**Figure 8.** Edge fracture pattern and locations on blanked edges for (a) DP1000 and (b) QP1000 with blue marks for minor cracks, (c) further expanded with four major cracks at the punched edge of DP1000, and (d) QP1000.

*3.2.4. Damage mechanism analysis of the fractured specimens.*

The SEM fractography of the local critical area in the section close to the fracture surface after uniaxial tensile tests are shown in Figure 9 (a), with the red quadrilaterals and blue circles indicating micro-cracks and voids, respectively. The number of defects, in terms of voids and micro-cracks, is distinctively larger in QP1000 than in DP1000, especially for voids. It is noticeable that both ferrite and martensite grains are extremely elongated in the severe deformation zone in DP1000, as previously reported [27]. For DP steels, three void nucleation damage mechanism modes including martensite brittle cracking, ferrite-martensite interface decohesion, and ferrite-ferrite grain boundary decohesion are commonly found. Since both phases are relatively fine microstructures, it is difficult to distinguish between microcracks and voids from the phase boundaries. However, as the ferrite phase shows generally higher ductility and deformed more easily compared to martensite, phase boundary debonding is the main failure type under tensile loading at room temperature [27], while for higher temperatures, more complex damage mechanisms take place due to dynamic strain aging effects [28]. The current investigated QP grade contains both tempered martensite and secondary martensite, arising the fraction of the harder and more brittle phases in general. In addition, the interaction between RA and martensite in QP steels exacerbates the occurrence of phase boundary debonding during uniaxial tension, leading to the formation of voids and cracks more easily to reach rupture.

The deformation history of both materials, including the plastic localization, damage initiation, and fracture can be found in the schematic drawing from Figure 9 (b). QP1000 shows a higher uniform deformation strain than DP1000. DP1000 yields a large amount of plastic localization before damage occurs followed by a fast damage evolution stage until the final fracture. While QP steels exhibit low resistance to fracture due to their sensitivity to damage development, resulting in lower local formability. In DP1000, damage concentrates on localized regions. QP1000 on the other hand has a more homogeneous deformation with more uniformly distributed damage. However, with a larger amount of voids and micro-cracks, the rather uniform deformation and uniform damage distribution lead to a sudden fracture with the cracks growing along. In contrast, the high level of strain localization and corresponding concentrated damage of DP1000 leads to a fracture pattern with significant necking.

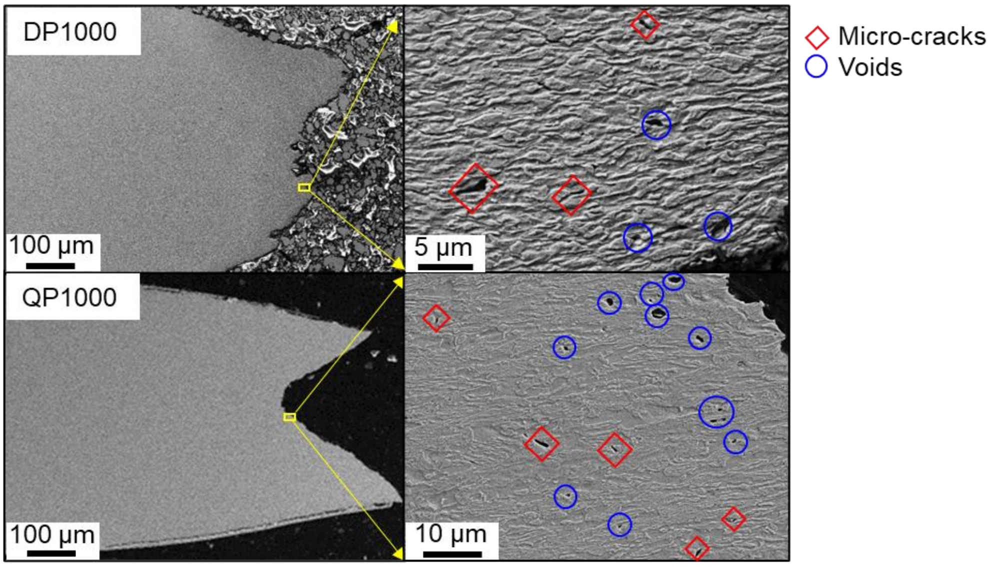


(a)

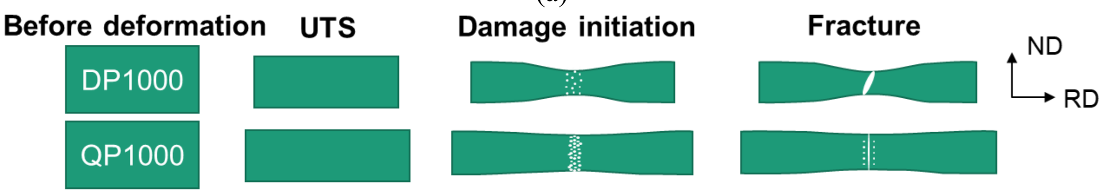


(b)

**Figure 9.** Microstructure-level damage mechanism analysis: (a) SEM fractography of fractured specimens with the red and blue indicators pointing out the micro-cracks and voids, respectively, and (b) schematic drawing of the relationship pattern during uniaxial tension for DP1000 and QP1000.

## 4. Conclusions

(1) The QP1000 steel in this study has an enhanced global formability with yield strength over 750 MPa and a superior total elongation of about 25%, while the local formability is conservatively proved by the hole expansion ratio of 62% for the smooth edge and 21% for the blanked edge.
(2) The DP1000 steel in this study shows satisfied tensile properties with a yield strength of 770 MPa and a moderate total elongation of 11%, while the local formability is promoted with a relatively high hole expansion ratio of 92% for the smooth edge and 29% for the blanked edge.
(3) The surface condition plays a dominant role in the edge formability and the formability reduces severely from machined hole to blanked hole for both materials in 66-68%.
(4) DP1000 demonstrates superior local formability with higher damage tolerance and edge fracture resistance due to fewer micro-cracks and local voids generated along deformation, while, despite the superior global formability and strain hardening rate, QP1000 exhibits strong sensitivity to damage with more micro defects during deformation due to its more complex microstructure, therefore limiting the local formability.

## References

[1] Bouaziz O, Zurob H and Huang M 2013 Driving force and logic of development of advanced high strength steels for automotive applications *Steel Res Int* **84** 937-47
[2] Rana R and Singh S B 2016 *Automotive steels: design, metallurgy, processing and applications*: Woodhead Publishing)
[3] Tsipouridis P, Werner E, Krempaszky C and Tragl E 2006 Formability of High Strength Dual-phase Steels *Steel Res Int* **77** 654-67
[4] Lian J, Liu P and Münstermann S 2012 Modeling of damage and failure of dual phase steel in Nakajima test *Key Engineering Materials* **525-526** 69-72
[5] Lian J, Sharaf M, Archie F and Münstermann S 2013 A hybrid approach for modelling of plasticity and failure behaviour of advanced high-strength steel sheets *International Journal of Damage Mechanics* **22** 188-218
[6] Wu-Rong W, Chang-Wei H, Zhong-Hua Z and Xi-cheng W 2011 The limit drawing ratio and formability prediction of advanced high strength dual-phase steels *Materials & Design* **32** 3320-7
[7] Hance B 2016 Advanced high strength steel: Deciphering local and global formability. In: *Proc. International Automotive Body Congress, Dearborn, MI,* p 2
[8] Westhäuser S, Schneider M, Teschner M and Denks I 2019 Local ductility–key parameter for predicting formability of AHSS. In: *IOP Conference Series: Materials Science and Engineering*: IOP Publishing) p 012049
[9] Speer J, Matlock D K, De Cooman B C and Schroth J 2003 Carbon partitioning into austenite after martensite transformation *Acta Mater* **51** 2611-22
[10] Chen X, Niu C, Lian C and Lin J 2017 The evaluation of formability of the 3rd generation advanced high strength steels QP980 based on digital image correlation method *Procedia Engineer* **207** 556-61
[11] Feistle M, Golle R and Volk W 2022 Edge crack test methods for AHSS steel grades: A review and comparisons *J Mater Process Tech* **302** 117488
[12] Leu D-K, Chen T-C and Huang Y-M 1999 Influence of punch shapes on the collar-drawing process of sheet steel *J Mater Process Tech* **88** 134-46
[13] Huang Y-M and Chien K 2002 Influence of cone semi-angle on the formability limitation of the hole-flanging process *The International Journal of Advanced Manufacturing Technology* **19** 597-606
[14] Xu L, Chen L, De Cooman B, Steglich D and Barlat F 2010 Hole expansion of advanced high strenth steel sheet sample *International Journal of Material Forming* **3** 247-50
[15] Larour P, Freudenthaler J, Kerschbaum M and Dolzer D 2020 Edge crack sensitivity versus tensile local ductility of AHSS sheet steels. In: *IOP Conference Series: Materials Science and Engineering*: IOP Publishing) p 012080

IOP Conf. Series: Materials Science and Engineering 1284 (2023) 012021 doi:10.1088/1757-899X/1284/1/012021

[16] Pathak N, Butcher C and Worswick M 2016 Assessment of the critical parameters influencing the edge stretchability of advanced high-strength steel sheet *Journal of Materials Engineering and Performance* **25** 4919-32
[17] Chiriac C and Chen G 2008 Local formability characterization of AHSS–Digital camera based hole expansion test development. In: *IDDRG 2008 Conference,* pp 16-8
[18] Wang K, Luo M and Wierzbicki T 2014 Experiments and modeling of edge fracture for an AHSS sheet *Int J Fracture* **187** 245-68
[19] Mu L, Wang Y, Zang Y and Araujo Stemler P M 2017 Edge Fracture Prediction Using Uncoupled Ductile Fracture Models for DP780 Sheet *Journal of Failure Analysis and Prevention* **17** 321-9
[20] Madrid M, Van Tyne C, Sriram S, Pavlina E, Hu J and Clarke K 2018 Hole expansion ratio in intercritically annealed QP 980/1180 steel grades as a function of testing condition. In: *IOP Conference Series: Materials Science and Engineering*: IOP Publishing) p 012083
[21] Goshert B, Terrazas O, Matlock D and Van Tyne C 2018 Sample edge effects on tensile properties and sheet formability. In: *IOP Conference Series: Materials Science and Engineering*: IOP Publishing) p 012064
[22] Shen F, Wang H, Liu Z, Liu W, Könemann M, Yuan G, Wang G, Münstermann S and Lian J 2022 Local formability of medium-Mn steel *J Mater Process Tech* **299** 117368
[23] Liu W, Lian J, Aravas N and Münstermann S 2020 A strategy for synthetic microstructure generation and crystal plasticity parameter calibration of fine-grain-structured dual-phase steel *International Journal of Plasticity* **126** 102614
[24] Chang Y 2021 *Evidence and effects of heterogeneities in complex phase and dual phase steels* Dissertation RWTH Aachen University Aachen, Germany
[25] Li Z, Chang Y, Liu W and Lian J 2023 Predicting edge fracture in dual-phase steels: significance of anisotropy-induced localization *under review*
[26] Misra R, Thompson S, Hylton T and Boucek A 2001 Microstructures of hot-rolled high-strength steels with significant differences in edge formability *Metallurgical and Materials Transactions A* **32** 745-60
[27] Liu W, Lian J and Münstermann S 2019 Damage mechanism analysis of a high-strength dual-phase steel sheet with optimized fracture samples for various stress states and loading rates *Engineering Failure Analysis* **106** 104138
[28] Liu W and Lian J 2021 Stress-state dependence of dynamic strain aging: Thermal hardening and blue brittleness *International Journal of Minerals, Metallurgy and Materials* **28** 854-66